ACS Energy LETTERS

Cite This: ACS Energy Lett. 2018, 3, 1233−1240

LETTER

Highly Crystalline Methylammonium Lead Tribromide Perovskite Films for Efficient Photovoltaic Devices

Nakita K. Noel,*[,†,‡] Bernard Wenger,[†] Severin N. Habisreutinger,[†,§] Jay B. Patel,[†] Timothy Crothers,[†] Zhiping Wang,[†] Robin J. Nicholas,[†] Michael B. Johnston,[†] Laura M. Herz,[†] and Henry J. Snaith*[,†]

[†]Clarendon Laboratory, Department of Physics, University of Oxford, Parks Road, Oxford OX1 3PU, U.K.

[‡]Department of Electrical Engineering, Princeton University, 41 Olden Street, Princeton, New Jersey 08544, United States

Supporting Information

ABSTRACT: The rise of metal-halide perovskite solar cells has captivated the research community, promising to disrupt the current energy landscape. While a sizable percentage of the research done on this class of materials has been focused on the neat and iodide-rich perovskites, bromide-based perovskites can deliver substantially higher voltages because of their relatively wide band gaps of over 2 eV. The potential for efficient, high-voltage devices makes materials such as these incredibly attractive for multijunction photovoltaic applications. Here, we use the acetonitrile/methylamine solvent system to deposit smooth, highly crystalline films of $CH_3NH_3PbBr_3$. By using choline chloride as a passivating agent for these films, we achieve photoluminescence quantum efficiencies of up to 5.5% and demonstrate charge-carrier mobilities of 17.8 $cm^2/(V\,s)$. Incorporating these films into photovoltaic devices, we achieve scanned power conversion efficiencies of up to 8.9%, with stabilized efficiencies of 7.6%, providing a simple route to realizing efficient, high-voltage $CH_3NH_3PbBr_3$ planar-heterojunction devices.

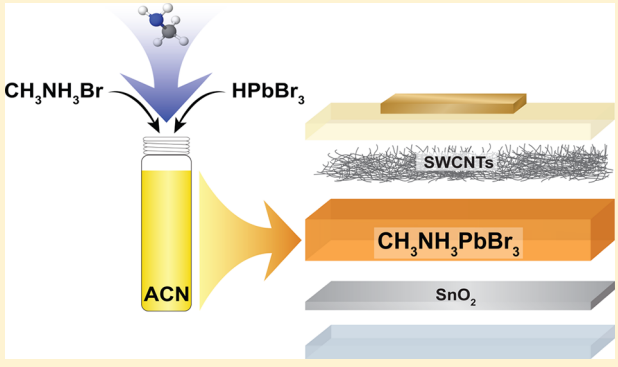

Metal halide perovskites have amassed tremendous interest over the last five years, largely due to the impressive power conversion efficiencies (PCEs) that have been achieved with perovskite-based solar cells.[1,2] In a relatively short period of time, the PCEs of lead halide perovskite solar cells have soared from 3.8%[3] to a certified 22.1%.[4] This rapid increase in PCE can largely be attributed to the development and application of improved deposition techniques, as well as careful tuning of the perovskite composition and stoichiometry.

Most of the research effort has been focused on the methylammonium lead triiodide ($CH_3NH_3PbI_3$) and formamidinium lead triiodide ($HC(NH_2)_2PbI_3$), or iodide-rich, mixed cation, and mixed halide perovskites. Indeed, the highest efficiency perovskite solar cells utilize the more thermally stable $HC(NH_2)_2PbI_3$ with inclusions of small amounts of Cs^+, Br^-, and $CH_3NH_3^+$ to provide structural stability, and to further increase the thermal stability of the material.[5−7] Comparatively little effort has been placed on the development of the neat bromide, and bromide-rich compositions of lead-based perovskites, likely because of their larger band gaps, which are less ideal for high-efficiency single-junction solar cells. While the band gaps of the neat iodide and the iodide-rich compositions of lead-based perovskites are very close to ideal for single-junction solar cells, the wider band gap bromide-based perovskites (E_g > 2.0 eV) are promising candidates for implementation in perovskite-based tandem and triple-junction solar cells.[8]

A metric with which to assess the fundamental energy loss in a photovoltaic device is to estimate the difference in energy between the band gap of the absorber layer (the lowest energy at which photons are absorbed) and the open-circuit voltage (V_{OC}) that the solar cell generates under full sunlight. In an ideal solar cell, this "loss-in-potential" or "voltage deficit" is in the range of 300 mV. While the band gap of the $HC(NH_2)_2PbBr_3$ and $CH_3NH_3PbBr_3$ perovskites are approximately 2.2 to 2.3 eV, the highest voltage that has been reported for these systems is 1.61 V.[9] This makes the loss-in-potential for the neat bromide perovskite devices >600 mV, which is almost twice as large as the 360 mV achieved for the iodine-rich perovskite cells.[10−12] A variety of reasons for this increased voltage loss have been postulated, one of which is an

Received: March 28, 2018
Accepted: April 30, 2018

DOI: 10.1021/acsenergylett.8b00509
ACS Energy Lett. 2018, 3, 1233−1240

unfavorable alignment between the highest occupied molecular orbital (HOMO) of the more commonly used hole-transporting materials such as spiro-OMeTAD.[13] In some of the early work on $CH_3NH_3PbBr_3$ solar cells, efficient devices were obtained by using a triarylamine polymer derivative (PIF8-TAA) in place of spiro-OMeTAD in the conventional n-i-p configuration. This was done using both mesoporous and planar TiO_2, resulting in PCEs of 6.7%[13] and 10.4%,[14] respectively, with corresponding open-circuit voltages of 1.4 and 1.51 V.

More recently, $CH_3NH_3PbBr_3$ has been employed in the p-i-n device configuration, and the same approach has been applied to the electron extraction layers (ETLs).[9,15] Indene-C_{60} bisadduct (ICBA) possesses a lowest unoccupied molecular orbital (LUMO) level closer to vacuum than phenyl-C_{61}-butyric acid methyl ester (PCBM), a member of the family of fullerene derivatives that is widely used in the fabrication of perovskite solar cells. By replacing PCBM with ICBA in the p-i-n cell structure, Wu et al. have reported a record high voltage of 1.61 V for $CH_3NH_3PbBr_3$-based solar cells. This increase in voltage has been attributed to a combination of both the better positioned LUMO of ICBA, as well as it passivating the grain boundaries in the perovskite film.[9]

The rapid crystallization of the bromide-based perovskites makes it nontrivial to obtain high-quality, smooth, pinhole-free films.[10,11] While a great deal of research has been focused on improving the quality of the lead iodide-based perovskite films,[16−18] comparatively little effort has been placed on improving the quality of the lead bromide-based films. Most of the early work done on bromide-based solar cells was either done on mesoporous films, which allowed for complete coverage,[10,11,14] or were directly tailored to improving the crystallization of films, thus controlling the extent of the available shunting pathways.[10,14,19] Efficient, planar heterojunction bromide devices have also been fabricated using a two-step deposition method[9,19,20] as well as the antisolvent quenching approach.[15] We have recently developed a solvent system that enables the deposition of high-quality, uniform, pinhole free $CH_3NH_3PbI_3$ films.[21] In this work, we extend the use of this solvent system to the $CH_3NH_3PbBr_3$ perovskite and find that it yields films with increased crystallinity and uniformity, as compared to those produced from the traditional DMF-based solvent, yielding efficient planar heterojunction solar cells with efficiencies of over 7%, and a maximum open-circuit voltage of 1.52 V.

We have recently shown that amines can be used in conjunction with polar, aprotic solvents such as acetonitrile (ACN) to facilitate the dissolution of $CH_3NH_3PbI_3$ perovskite precursor salts.[21] However, this dissolution process cannot be directly translated to $CH_3NH_3PbBr_3$, as it results in an unstable precursor solution. Here, using a modified process, we disperse $CH_3NH_3PbBr_3$ precursor salts in ACN and saturate the solution with methylamine (MA) gas, resulting in the dissolution of the precursor salts to obtain a stable, clear, colorless solution (see Materials and Methods in the Supporting Information). Upon spin-coating this solution, we obtain a smooth, dense film that has the characteristic orange color of $CH_3NH_3PbBr_3$. While films of $CH_3NH_3PbBr_3$ are known to crystallize very rapidly from more conventional solvents such as *N*,*N*-dimethylformamide (DMF), this rapid crystallization often comes at the expense of film quality. For DMF there usually exists many highly oriented, large crystals randomly distributed over the substrate, resulting in a high density of pinholes in the film.[10,14] It has previously been reported that by adding hydrobromic acid (HBr) to the solution, the crystallization kinetics are changed, such that a smooth, dense film with uniform coverage can be obtained.[14] In Figure S1 we show microscopy images of films we have obtained from both neat DMF and DMF with the addition of HBr. Here, we see that without the addition of the acid, there are large, individual crystalline domains on the substrate. When the acid is added to the DMF, these crystals become smaller and appear to be more highly oriented. However, even at the high concentration of 100 μL/mL, we are unable to achieve a uniform film with complete substrate coverage. In contrast, when deposited from the ACN/MA compound solvent, we find that the resulting film comprises what appears to be large, flat grains which fully impinge upon each other and contain far fewer pinholes. We show the scanning electron microscopy (SEM) images in Figure 1.

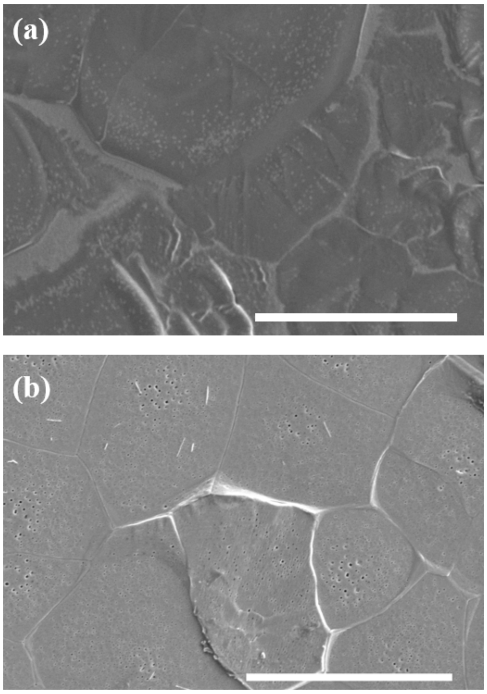

Figure 1. Microscopy images. SEM images of $CH_3NH_3PbBr_3$ deposited from (a) neat DMF and (b) the ACN/MA compound solvent. Scale bars represent a distance of 10 μm.

From the SEM images in Figure 1, it appears that films deposited from the ACN/MA solvent not only are smoother but also maintain appreciably large grain sizes. This is in agreement with our previous observations made on the iodide-based system, that the rapid crystallization which occurs as a result of the low boiling point solvent, does not result in a loss of crystallinity in the film.[21] Interestingly, we find that the films processed from the ACN/MA solvent appear to have small holes in the crystal, which through analysis of cross-sectional SEM images (which we show in the Supporting Information) appear to be only on the surface of the film. While the exact cause for these is unknown, we postulate that they may be generated because of the evaporation of residual solvent which may have been trapped in the film during the rapid crystallization process. Upon heating, this solvent may evaporate, causing small physical cavities on or near the surface of the crystals.

DOI: 10.1021/acsenergylett.8b00509
ACS Energy Lett. 2018, 3, 1233−1240

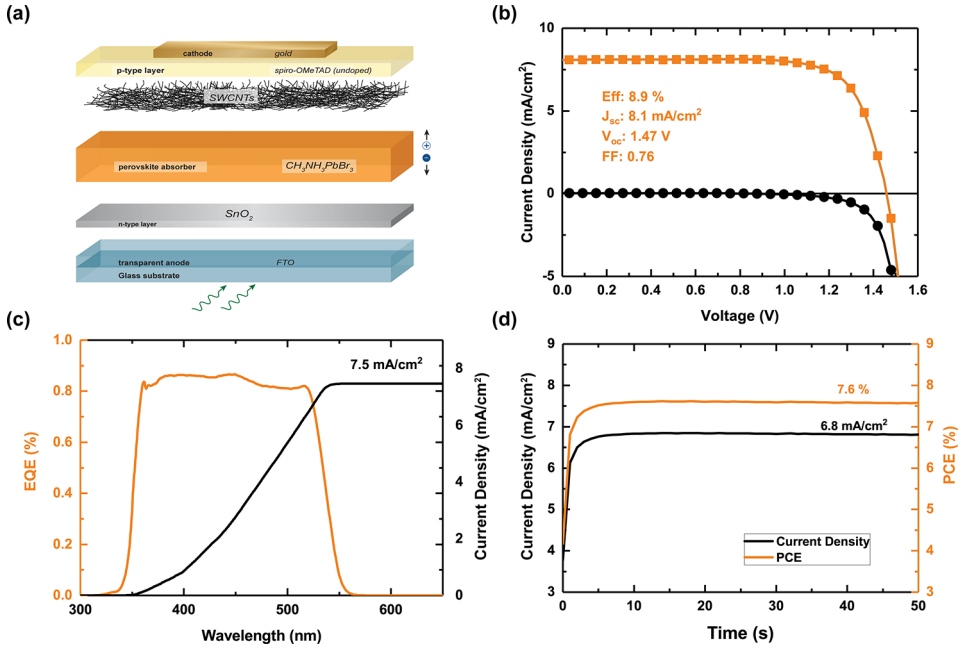

Figure 2. X-ray diffractograms. Powder and 2D X-ray diffractograms of (a and b) $CH_3NH_3PbBr_3$ deposited from DMF and (c and d) $CH_3NH_3PbBr_3$ deposited from ACN/MA.

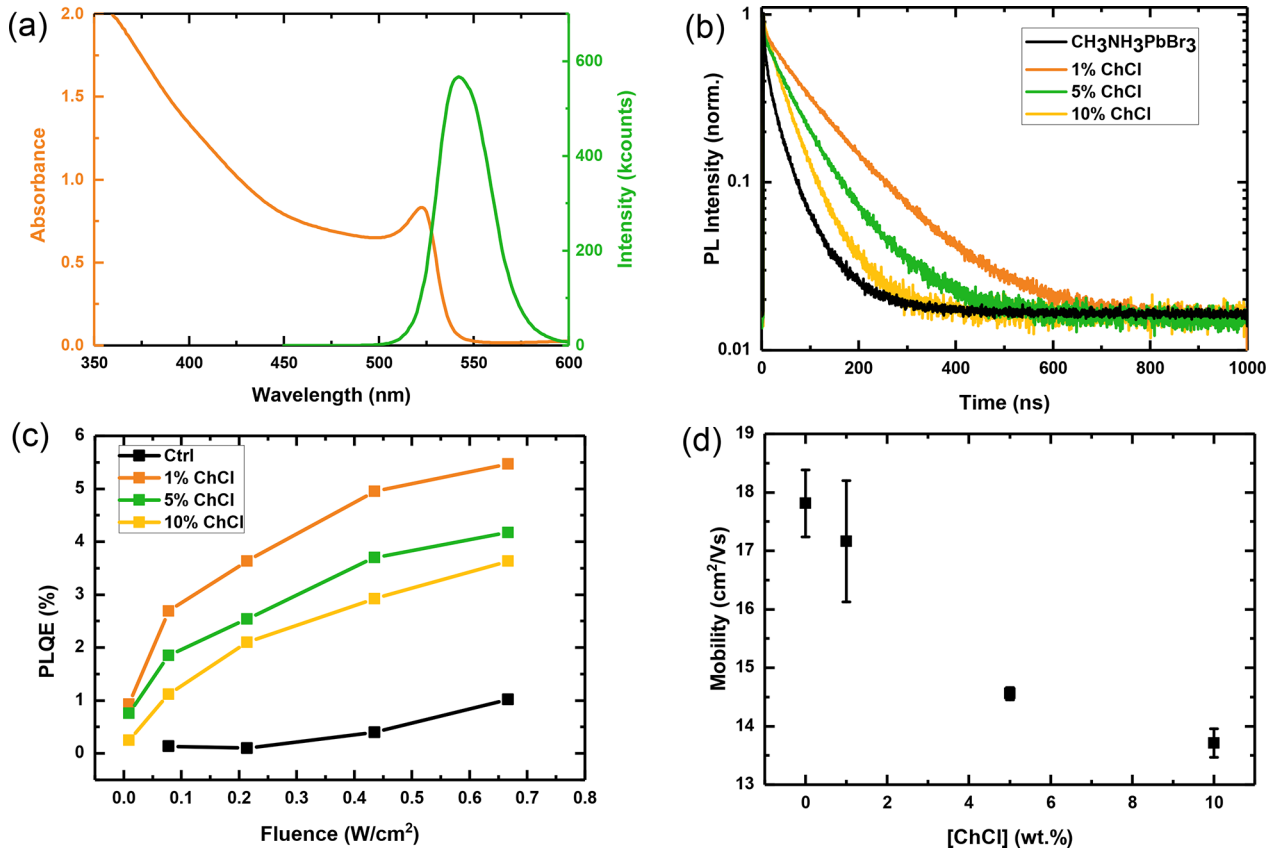

Figure 3. Optical measurements. (a) Absorbance and steady-state photoluminescence (PL) of a thin film of $CH_3NH_3PbBr_3$. (b) PL decays of a neat $CH_3NH_3PbBr_3$ film and $CH_3NH_3PbBr_3$ films treated with choline chloride (ChCl). Film samples were photoexcited using a 405 nm laser head (LDH-P-C-405, PicoQuant GmbH) pulsed at frequencies between 0.3 and 10 MHz, with a pulse duration of 117 ps and fluence of ~30 nJ/cm². (c) Fluence-dependent PL quantum efficiencies of neat and ChCl-treated films of $CH_3NH_3PbBr_3$. (d) Charge-carrier mobilities of neat and ChCl-treated films of $CH_3NH_3PbBr_3$, as measured by terahertz photoconductivity spectroscopy.

Next, we investigate the crystal structure and the degree of crystallinity of these films by performing X-ray diffraction (XRD) measurements. In Figure 2 we present the results of both the powder and two-dimensional (2D) diffraction scans.

DOI: 10.1021/acsenergylett.8b00509
ACS Energy Lett. 2018, 3, 1233−1240

In panels a and c of Figure 2 we show the powder diffraction patterns of $CH_3NH_3PbBr_3$ films deposited from DMF and ACN/MA, respectively. For the films processed from both solvents, all the reflections can be assigned to the cubic $CH_3NH_3PbBr_3$ perovskite phase.[22] Interestingly, we see that the intensity of the (100) peak increases by approximately 2 orders of magnitude for the films deposited from the ACN/MA compound solvent. We note that films deposited from the two routes have very similar thicknesses (380−400 nm), and as such the differences in peak intensity cannot be attributed to a difference in film thickness. We believe that this increase in the peak intensity occurs because of increased texturing and grain orientation in the film deposited from the compound solvent. To gain more information on the crystallographic orientation in both these films, we performed a two-dimensional XRD (2D-XRD) measurement. The 2D hybrid pixel array detector employed in this measurement allows us to measure complete Debye−Scherrer cones.[5] We show the 2D-XRD images in Figure 2b,d. We observe two major reflections located at q_z = 1 and 2 Å, which correspond to the (100) and (200) reflections of the $CH_3NH_3PbBr_3$, respectively. The film deposited from DMF displays intense diffraction patterns along the specular direction. At the same time, we also notice many weak reflections across the entire arc. Figure S2 displays the integrated (100) peak intensity in the azimuthal direction (i.e., intensity vs β). For the film deposited from DMF, we can clearly observe two broad peaks at β = 120° and 240° in addition to the major peak at β = 180°. In contrast, for the film deposited from the ACN/MA solvent, most of the (100) reflections appear in the specular direction and are distributed at β = 180° with a much higher intensity in the scattering intensity versus β plot. This confirms that the perovskite film processed from the ACN/MA solvent has a much higher degree of texture than the film deposited from DMF.

Despite the remarkable device performances that have been achieved using perovskite materials, it is well-established that there are defect states present in polycrystalline films.[23,24] These defects are thought to occur mostly at the grain boundaries, taking the form of halide or alkylammonium vacancies. We, and others, have previously shown that Lewis bases such as thiophene and pyridine can be used to passivate trap states on the surface of perovskite films through coordination to undercoordinated Pb.[25,26] However, this methodology is not sufficient to passivate any defects that may exist because of the presence of alkylammonium vacancies. Recently, quaternary ammonium halides have been used as surface treatments for perovskite films with the aim of passivating two potential defects sites with one molecule.[27,28] Indeed, the use of these materials has been shown to reduce nonradiative recombination and the energetic disorder in polycrystalline perovskite films.

Having determined that the $CH_3NH_3PbBr_3$ films deposited from the compound solvent have both superior surface coverage and increased crystallinity, we then move on to assess the optoelectronic quality of these films through a series of optical measurements. We show the results of these investigations in Figure 3. In Figure 3a we show the absorbance and the PL emission of a $CH_3NH_3PbBr_3$ film. We observe the characteristic excitonic absorption onset at 540 nm, with the corresponding PL emission centered around 542 nm. Films of $CH_3NH_3PbBr_3$ have been shown to have PL lifetimes significantly shorter than those of their single-crystal counterparts.[29,30] While the reason for this is still largely unknown, it may be the result of defects at the grain boundaries of individual crystals which make up a polycrystalline film. Here, we attempt to passivate any defects which may be present at the grain boundaries through a post-treatment with a quaternary ammonium halide salt, choline chloride (ChCl).[27] We investigate the effect of the ChCl by examining the photoluminescence (PL) decays as well as the photoluminescence quantum efficiency (PLQE) of the control and passivated $CH_3NH_3PbBr_3$ films. In general, a longer PL lifetime or higher PLQE indicates the presence of long-lived carrier species and a reduction of nonradiative recombination within the film, which is one of the main loss pathways for charge carriers in optoelectronic devices. The PL decays are characterized by a very fast drop during the first tens of nanoseconds, which has been attributed to either inhomogeneity within the films and/or diffusion of carriers within the film.[30,31] This is followed by a slower decay phase which follows a nearly monoexponential rate. We fit the longer time slow component of the decays with a monoexponential function and extract lifetimes. For the 1% ChCl treated sample, we observe a significant increase in the PL lifetime, from 47 ns for the control film to 111 ns for the 1% ChCl treated sample. However, upon further increasing the ChCl concentration, we observe a steady decrease in the PL lifetime, to 79 and 51 ns for the 5% ChCl and 10% ChCl treated samples, respectively (see Figure S3). For the PLQE, which we show in Figure 3c, we observe an increase with respect to the control, for all the ChCl-treated films. Notably, we estimate a PLQE increase from 1.0% to 5.5% for the lowest-concentration ChCl treatment, suggesting that the use of this treatment acts to inhibit nonradiative recombination processes in the $CH_3NH_3PbBr_3$ perovskite. We have recently discussed the optical properties of large single crystals of $CH_3NH_3PbBr_3$ and measured external PLQEs of up to 6.0%.[30] With the use of the ChCl surface treatment on our thin films, we find that we can achieve PLQEs approaching that of our best single crystals, indicating improved optoelectronic quality. We do acknowledge, however, that self-absorption effects more strongly limit optical out-coupling in large single crystals, indicating that the internal luminescence quantum yield of our films will still be lower than that of the single crystals. Furthermore, we observe that with increasing concentration of ChCl, there is a blue-shift in the absorption onset. This is likely to be due to the incorporation of a small fraction of the Cl^- ions into the perovskite structure.[11,32] We show the absorption spectra of these films in Figure S4.

From the data shown in Figure S4, we observe a negligible change in the absorption onset when the $CH_3NH_3PbBr_3$ films are treated with 1% ChCl but a significant blueshift when the films are treated with 5−10% ChCl. This suggests that while at 1% ChCl the dominant effect is the passivation of surface states in the material, when treated with a higher concentration of ChCl, a significant percentage of the Cl^- ions are incorporated into the perovskite structure, effectively changing the bulk composition of the material. To isolate the effect of the chloride ions, we treat the surface of the $CH_3NH_3PbBr_3$ films with a solution of CH_3NH_3Cl of equivalent molarities to the ChCl solutions. We present the absorbance and PL decays of these films in Figure S5. From these results we see that at low concentrations of the CH_3NH_3Cl treatment there is no meaningful change in the absorption onset or lifetime of the perovskite film. However, at higher concentrations of CH_3NH_3Cl where, as evidenced by the noticeable blueshift in the absorption onset, incorporation of the Cl^- ions into the

DOI: 10.1021/acsenergylett.8b00509
ACS Energy Lett. 2018, 3, 1233−1240

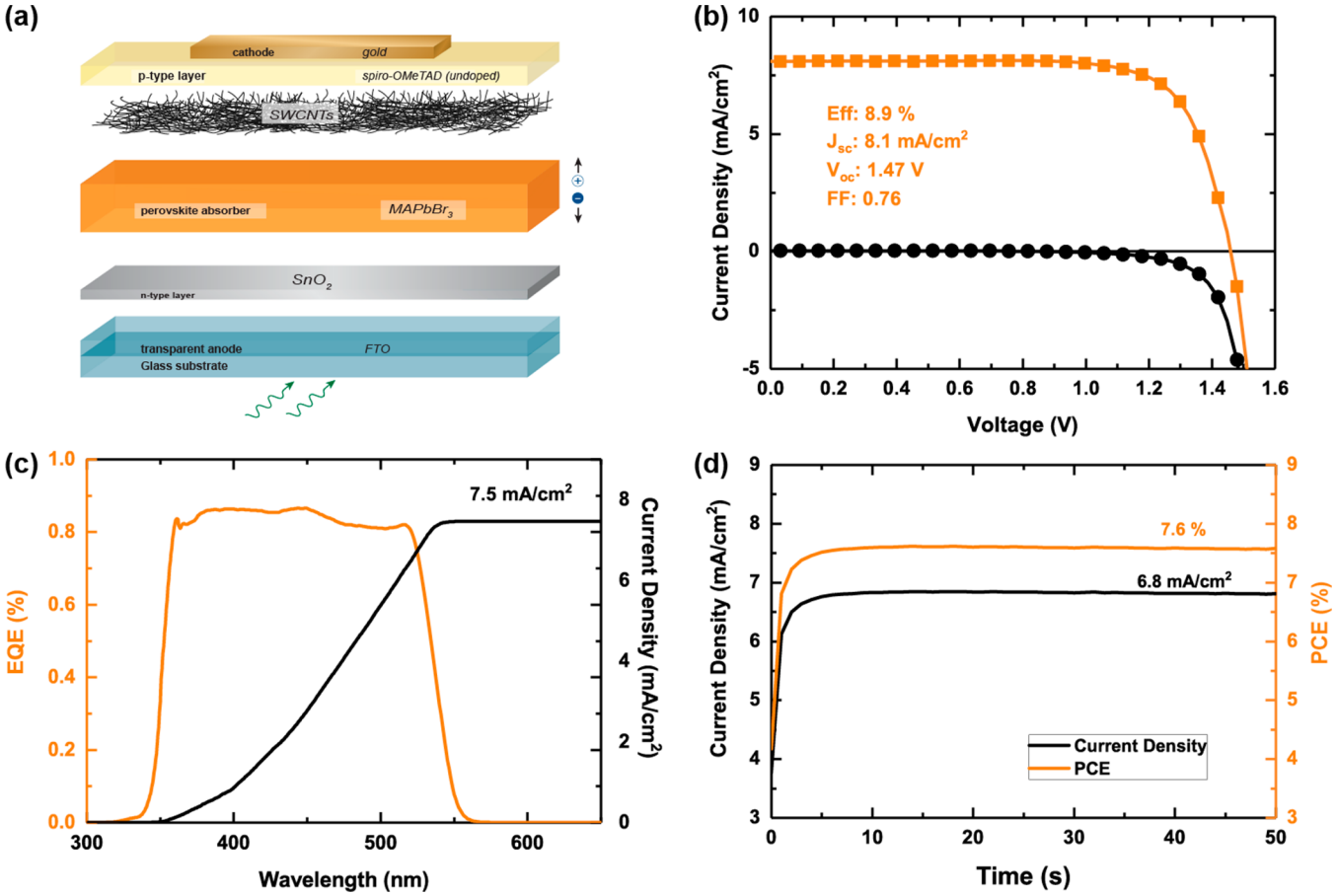

Figure 4. Device results. (a) Schematic of the device architecture employed. (b) Current–voltage curves of the champion $CH_3NH_3PbBr_3$ device. (c) External quantum efficiency (EQE) of the device shown in panel b. (d) Steady-state current and PCE of the champion device shown in panel b.

structure occurs, there is a quenching of the PL lifetimes, indicative of an increase in the density of trap states in the material. This indicates that the improvement in the optoelectronic quality of the $CH_3NH_3PbBr_3$ films which results from the ChCl surface treatment is in fact due to the passivation of trap states, rather than the incorporation of Cl^- to form a mixed halide perovskite composition.

We further probe the films by use of optical-pump terahertz-probe spectroscopy to determine the charge-carrier mobility in both neat and ChCl-treated $CH_3NH_3PbBr_3$ films. It has previously been shown that bromide perovskites show stronger Fröhlich coupling than their iodide counterparts, fundamentally limiting charge-carrier mobility, and as such, we expect the charge-carrier mobility of the bromide-based perovskites to be significantly lower.[33] For example, using Hall effect and resistivity measurements, hole mobilities of 40 $cm^2/(V\,s)$ and 105 $cm^2/(V\,s)$ were obtained for single crystals of $CH_3NH_3PbBr_3$ and $CH_3NH_3PbI_3$, respectively.[34−36] While charge-carrier mobilities for films of the formamidinium and formamidinium-cesium bromide perovskites have previously been determined,[37,38] to the best of our knowledge, there are no reports in which the carrier mobility in thin films of $CH_3NH_3PbBr_3$ has been directly measured. From our measurements, we determine the charge carrier mobility in the neat $CH_3NH_3PbBr_3$ film deposited from ACN/MA to be 17.8 ± 0.6 $cm^2/(V\,s)$, which is slightly higher than the mobilities reported for the neat $HC(NH_2)_2PbBr_3$ perovskite (14 $cm^2/(V\,s)$) processed from a DMF solvent.[38] Interestingly, when the ChCl is deposited onto the film at a low concentration (1%), the mobility appears to be largely unchanged (17.1 ± 1.0 $cm^2/(V\,s)$); however, as we increase the concentration, we observe the mobility to decrease to 13.7 $cm^2/(V\,s)$ (Figure 3d). From the charge-carrier mobilities and the lifetimes we can estimate the diffusion lengths of the free carriers, which range between 1.3 μm (ChCl 10%) and 2.2 μm (ChCl 1%) for the treated films and 1.5 μm for the untreated films.[34] A summary of the data obtained from the optical measurements as well as details on the estimation of the diffusion length are provided in the Supporting Information (Table S1). Such long diffusion lengths should allow for the efficient extraction of charges in photovoltaic devices, with absorber layers which are sufficiently thick to absorb most of the supra band gap solar irradiation. The combination of these optical measurements definitively shows that there is a beneficial effect of using a low concentration of ChCl as a surface treatment, in that it reduces the degree of nonradiative recombination in the film without negatively affecting the charge carrier mobility, while an increased concentration of the ChCl seems to reintroduce charge recombination pathways and effectively reduces the charge-carrier mobility.

Having shown that with the use of the compound ACN/MA solvent we are able to produce $CH_3NH_3PbBr_3$ films with increased surface coverage and improved crystallinity, and that by using a surface treatment with ChCl we are able to reduce nonradiative recombination in these films, we proceed to investigate how the films of the best quality (where the

DOI: 10.1021/acsenergylett.8b00509
ACS Energy Lett. 2018, 3, 1233−1240

perovskite is treated with 1% ChCl) perform when incorporated into a photovoltaic device. In this work we use the n-i-p device architecture with single-walled carbon nanotubes (SWCNTs) interpenetrated with spiro-OMeTAD as the hole extraction layer (FTO/SnO_2/$CH_3NH_3PbBr_3$/SWCNT/spiro-OMeTAD/Au). This architecture has previously been employed to obtain efficient mixed-cation, mixed-halide perovskite solar cells.[39] We present a schematic of the device architecture, along with the champion device results, in Figure 4 and a cross-sectional SEM image of a typical device, along with device performance parameter statistics, in Figures S6 and S7.

Consistent with previous reports on $CH_3NH_3PbBr_3$ solar cells, we observe significant hysteresis in the current−voltage (J−V) curves of these devices (see Figure S8).[20] Similar to the neat iodide and iodide-rich perovskite solar cells, the hysteresis in the J−V curves likely arises because of a combination of mobile ions and trap states (both at the grain boundaries and at the interfaces).[40] Likewise, we expect that the hysteresis observed in these devices can be significantly reduced through identification and implementation of improved charge-selective layers, as well as the further reduction of trap states in the material itself. By using this compound solvent we are able to consistently obtain devices with power conversion efficiencies above 7% and achieve a maximum J−V scanned efficiency of 8.9% and a steady-state efficiency of 7.6%. To corroborate the J−V-determined J_{sc} of 8.1 mA/cm^2, we integrate the external quantum efficiency (EQE) of this device and obtain 7.5 mA/cm^2, a value which is in close agreement. We have also been able to achieve a maximum V_{OC} of 1.52 V; however, we must note that this was not achieved in the best performing device (see Figure S9). From the diffusion lengths which we have estimated using the lifetime extracted from the PL decay, in combination with the mobility determined through terahertz measurements, one would expect the device performance to show a much more noticeable improvement with choline chloride treatments. It is worth noting that while choline chloride may improve the overall optoelectronic quality of the perovskite film through the reduction of nonradiative recombination, the limiting factor in this case may be due to how efficiently the charges are extracted, suggesting that the bottleneck for these devices might be the nature of the electron- and hole-selective contacts. This hypothesis is further consolidated by the absence of a dependence of V_{OC} with the concentration of choline chloride.

By fitting the tail of the EQE spectrum, we can determine the Urbach energy of the material. This parameter provides an estimate of the degree of electronic disorder at the band edge of the perovskite absorber material. Previous reports estimate the Urbach energy of $CH_3NH_3PbBr_3$ films to be between 17 and 19 meV.[41] From our measurements, we determine the Urbach energies of the champion control and 1% ChCl treated devices to be 17.2 ± 0.03 and 16.8 ± 0.04 meV, respectively (see Figure S10). Additionally, we observe that if the concentration of the choline chloride used to treat the perovskite surface exceeds 1%, there is a subsequent increase in the Urbach energy of the material, corresponding to a decrease in the J_{SC} of the devices (Figure S11). Typically, $CH_3NH_3PbBr_3$ devices exhibit a significantly larger V_{OC} deficit, the difference in energy between the band gap of the absorber layer and the V_{OC} generated under full sun illumination, compared to their iodide-based counterparts. Chen et al. have reported voltages of up to 1.53 V for $CH_3NH_3PbBr_3$ cells fabricated using the p-i-n structure and have suggested that the major cause of the V_{OC} limitation is not defects in the perovskite layer but a misalignment in energy levels between the perovskite and the n-type contacts.[15] While finding the most appropriate electron-selective layers for this material is an area that is currently under investigation, the improvements in film quality gained through this deposition route suggests that by finding appropriate electron-selective layers for this material, we should be able to further increase the performance of these devices to beyond 10%.

In summary, we have demonstrated the use of the ACN/MA compound solvent system as an alternative solvent for precursor salts of the $CH_3NH_3PbBr_3$ perovskite and have shown that by using this solvent, we can deposit uniform, highly crystalline, wide band gap perovskite films with excellent optoelectronic properties. By using a quaternary ammonium halide salt as a passivating agent, we present a method by which we can further improve the photoluminescence lifetime and quantum efficiency of bromide-based perovskite films to a maximum of 110 ns and 5.5%, respectively. Furthermore, we report a direct measurement of the effective charge carrier mobility of neat and passivated $CH_3NH_3PbBr_3$ films, achieving mobilities of up to 18 cm^2/(V s). By incorporating these films into photovoltaic devices, we achieve scanned power conversion efficiencies of up to 8.9%, with corresponding steady-state efficiencies of up to 7.6%. Through the extension of this relatively new solvent system to the $CH_3NH_3PbBr_3$ perovskite, we have presented a scalable route to the deposition of high-quality films, which when combined with an appropriate electron extraction layer, has the potential to greatly reduce the voltage losses in $CH_3NH_3PbBr_3$-based perovskite solar cells.

■ ASSOCIATED CONTENT

Supporting Information

The Supporting Information is available free of charge on the ACS Publications website at DOI: 10.1021/acsenergylett.8b00509.

Full experimental methods, optical microscopy and SEM images, XRD and absorption data, device performance statistics, and Urbach energies (PDF)

■ AUTHOR INFORMATION

Corresponding Authors

*E-mail: nnoel@princeton.edu.
*E-mail: henry.snaith@physics.ox.ac.uk.

ORCID

Nakita K. Noel: 0000-0002-8570-479X
Bernard Wenger: 0000-0001-9026-7064
Severin N. Habisreutinger: 0000-0001-5760-8744
Zhiping Wang: 0000-0002-3081-0472
Michael B. Johnston: 0000-0002-0301-8033
Laura M. Herz: 0000-0001-9621-334X
Henry J. Snaith: 0000-0001-8511-790X

Present Address

§S.N.H.: National Renewable Energy Laboratory, Chemistry and Nanoscience Center, 15013 Denver West Parkway, Golden, CO.

Notes

The authors declare no competing financial interest.

■ ACKNOWLEDGMENTS

This work was funded by the Engineering and Physical Sciences Research Council (EPSRC) program Grant EP/P02484X/1.

DOI: 10.1021/acsenergylett.8b00509
ACS Energy Lett. 2018, 3, 1233−1240

B.W. acknowledges funding from the European Commission via a Marie Skłodowska-Curie individual fellowship (REA Grant Number 706552-APPEL). S.N.H acknowledges support from the International Collaborative Energy Technology R&D Program of the Korean Institute of Energy Technology Evaluation and Planning (KETEP).

REFERENCES

(1) Lee, M. M.; Teuscher, J.; Miyasaka, T.; Murakami, T. N.; Snaith, H. J. Efficient Hybrid Solar Cells Based on Meso-Superstructured Organometal Halide Perovskites. *Science* **2012**, *338* (6107), 643−647.

(2) Kim, H.-S.; Lee, C.-R.; Im, J.-H.; Lee, K.-B.; Moehl, T.; Marchioro, A.; Moon, S.-J.; Humphry-Baker, R.; Yum, J.-H.; Moser, J. E.; et al. Lead Iodide Perovskite Sensitized All-Solid-State Submicron Thin Film Mesoscopic Solar Cell with Efficiency Exceeding 9%. *Sci. Rep.* **2012**, *2*, 591.

(3) Kojima, A.; Teshima, K.; Shirai, Y.; Miyasaka, T. Organometal Halide Perovskites as Visible-Light Sensitizers for Photovoltaic Cells. *J. Am. Chem. Soc.* **2009**, *131* (17), 6050−6051.

(4) Yang, W. S.; Park, B.-W.; Jung, E. H.; Jeon, N. J.; Kim, Y. C.; Lee, D. U.; Shin, S. S.; Seo, J.; Kim, E. K.; Noh, J. H.; et al. Iodide Management in Formamidinium-Lead-Halide−based Perovskite Layers for Efficient Solar Cells. *Science* **2017**, *356* (6345), 1376−1379.

(5) McMeekin, D. P.; Wang, Z.; Rehman, W.; Pulvirenti, F.; Patel, J. B.; Noel, N. K.; Johnston, M. B.; Marder, S. R.; Herz, L. M.; Snaith, H. J. Crystallization Kinetics and Morphology Control of Formamidinium−Cesium Mixed-Cation Lead Mixed-Halide Perovskite via Tunability of the Colloidal Precursor Solution. *Adv. Mater.* **2017**, *29* (29), 1607039.

(6) McMeekin, D. P.; Sadoughi, G.; Rehman, W.; Eperon, G. E.; Saliba, M.; Hörantner, M. T.; Haghighirad, A.; Sakai, N.; Korte, L.; Rech, B.; et al. A Mixed-Cation Lead Mixed-Halide Perovskite Absorber for Tandem Solar Cells. *Science (Washington, DC, U. S.)* **2016**, *351* (6269), 151−155.

(7) Saliba, M.; Matsui, T.; Seo, J.-Y.; Domanski, K.; Correa-Baena, J.-P.; Nazeeruddin, M. K.; Zakeeruddin, S. M.; Tress, W.; Abate, A.; Hagfeldt, A.; et al. Cesium-Containing Triple Cation Perovskite Solar Cells: Improved Stability, Reproducibility and High Efficiency. *Energy Environ. Sci.* **2016**, *9* (6), 1989−1997.

(8) Hörantner, M. T.; Leijtens, T.; Ziffer, M. E.; Eperon, G. E.; Christoforo, M. G.; McGehee, M. D.; Snaith, H. J. The Potential of Multijunction Perovskite Solar Cells. *ACS Energy Lett.* **2017**, *2* (10), 2506−2513.

(9) Wu, C.-G.; Chiang, C.-H.; Chang, S. H. A Perovskite Cell with a Record-High-Voc of 1.61 V Based on Solvent Annealed $CH_3NH_3PbBr_3$/ICBA Active Layer. *Nanoscale* **2016**, *8* (7), 4077−4085.

(10) Edri, E.; Kirmayer, S.; Cahen, D.; Hodes, G. High Open-Circuit Voltage Solar Cells Based on Organic−Inorganic Lead Bromide Perovskite. *J. Phys. Chem. Lett.* **2013**, *4* (6), 897−902.

(11) Edri, E.; Kirmayer, S.; Kulbak, M.; Hodes, G.; Cahen, D. Chloride Inclusion and Hole Transport Material Doping to Improve Methyl Ammonium Lead Bromide Perovskite-Based High Open-Circuit Voltage Solar Cells. *J. Phys. Chem. Lett.* **2014**, *5* (3), 429−433.

(12) Noel, N. K.; Congiu, M.; Ramadan, A. J.; Fearn, S.; McMeekin, D. P.; Patel, J. B.; Johnston, M. B.; Wenger, B.; Snaith, H. J. Unveiling the Influence of pH on the Crystallization of Hybrid Perovskites, Delivering Low Voltage Loss Photovoltaics. *Joule* **2017**, *1* (2), 328−343.

(13) Ryu, S.; Noh, J. H.; Jeon, N. J.; Chan Kim, Y.; Yang, W. S.; Seo, J.; Seok, S. Il. Voltage Output of Efficient Perovskite Solar Cells with High Open-Circuit Voltage and Fill Factor. *Energy Environ. Sci.* **2014**, *7* (8), 2614−2618.

(14) Heo, J. H.; Song, D. H.; Im, S. H. Planar CH3NH3PbBr3 Hybrid Solar Cells with 10.4% Power Conversion Efficiency, Fabricated by Controlled Crystallization in the Spin-Coating Process. *Adv. Mater.* **2014**, *26* (48), 8179−8183.

(15) Chen, S.; Hou, Y.; Chen, H.; Richter, M.; Guo, F.; Kahmann, S.; Tang, X.; Stubhan, T.; Zhang, H.; Li, N.; et al. Exploring the Limiting Open-Circuit Voltage and the Voltage Loss Mechanism in Planar $CH_3NH_3PbBr_3$ Perovskite Solar Cells. *Adv. Energy Mater.* **2016**, *6* (18), 1600132.

(16) Eperon, G. E.; Burlakov, V. M.; Docampo, P.; Goriely, A.; Snaith, H. J. Morphological Control for High Performance, Solution-Processed Planar Heterojunction Perovskite Solar Cells. *Adv. Funct. Mater.* **2014**, *24*, 151−157.

(17) Liu, M.; Johnston, M. B.; Snaith, H. J. Efficient Planar Heterojunction Perovskite Solar Cells by Vapour Deposition. *Nature* **2013**, *501* (7467), 395−398.

(18) Burschka, J.; Pellet, N.; Moon, S.-J.; Humphry-Baker, R.; Gao, P.; Nazeeruddin, M. K.; Gratzel, M. Sequential Deposition as a Route to High-Performance Perovskite-Sensitized Solar Cells. *Nature* **2013**, *499* (7458), 316−319.

(19) Hanusch, F. C.; Wiesenmayer, E.; Mankel, E.; Binek, A.; Angloher, P.; Fraunhofer, C.; Giesbrecht, N.; Feckl, J. M.; Jaegermann, W.; Johrendt, D.; et al. Efficient Planar Heterojunction Perovskite Solar Cells Based on Formamidinium Lead Bromide. *J. Phys. Chem. Lett.* **2014**, *5* (16), 2791−2795.

(20) Sheng, R.; Ho-Baillie, A.; Huang, S.; Chen, S.; Wen, X.; Hao, X.; Green, M. A. Methylammonium Lead Bromide Perovskite-Based Solar Cells by Vapor-Assisted Deposition. *J. Phys. Chem. C* **2015**, *119* (7), 3545−3549.

(21) Noel, N. K.; Habisreutinger, S. N.; Wenger, B.; Klug, M. T.; Horantner, M. T.; Johnston, M. B.; Nicholas, R. J.; Moore, D. T.; Snaith, H. J. A Low Viscosity, Low Boiling Point, Clean Solvent System for the Rapid Crystallisation of Highly Specular Perovskite Films. *Energy Environ. Sci.* **2017**, *10* (1), 145−152.

(22) Noh, J. H.; Im, S. H.; Heo, J. H.; Mandal, T. N.; Seok, S. Il. Chemical Management for Colorful, Efficient, and Stable Inorganic−Organic Hybrid Nanostructured Solar Cells. *Nano Lett.* **2013**, *13* (4), 1764−1769.

(23) Stranks, S. D.; Burlakov, V. M.; Leijtens, T.; Ball, J. M.; Goriely, A.; Snaith, H. J. Recombination Kinetics in Organic-Inorganic Perovskites: Excitons, Free Charge, and Subgap States. *Phys. Rev. Appl.* **2014**, *2* (3), 034007.

(24) Ball, J. M.; Petrozza, A. Defects in Perovskite-Halides and Their Effects in Solar Cells. *Nat. Energy* **2016**, *1*, 16149.

(25) Noel, N. K.; Abate, A.; Stranks, S. D.; Parrott, E. S.; Burlakov, V. M.; Goriely, A.; Snaith, H. J. Enhanced Photoluminescence and Solar Cell Performance via Lewis Base Passivation of Organic−Inorganic Lead Halide Perovskites. *ACS Nano* **2014**, *8* (10), 9815−9821.

(26) de Quilettes, D. W.; Vorpahl, S. M.; Stranks, S. D.; Nagaoka, H.; Eperon, G. E.; Ziffer, M. E.; Snaith, H. J.; Ginger, D. S. Impact of Microstructure on Local Carrier Lifetime in Perovskite Solar Cells. *Science (Washington, DC, U. S.)* **2015**, *348* (6235), 683−686.

(27) Zheng, X.; Chen, B.; Dai, J.; Fang, Y.; Bai, Y.; Lin, Y.; Wei, H.; Zeng, X. C.; Huang, J. *Defect Passivation in Hybrid Perovskite Solar Cells Using Quaternary Ammonium Halide Anions and Cations* **2017**, *2*, 17102.

(28) Naphade, R.; Zhao, B.; Richter, J. M.; Booker, E.; Krishnamurthy, S.; Friend, R. H.; Sadhanala, A.; Ogale, S. High Quality Hybrid Perovskite Semiconductor Thin Films with Remarkably Enhanced Luminescence and Defect Suppression via Quaternary Alkyl Ammonium Salt Based Treatment. *Adv. Mater. Interfaces* **2017**, *4* (19), 1700562.

(29) Yang, Y.; Yan, Y.; Yang, M.; Choi, S.; Zhu, K.; Luther, J. M.; Beard, M. C. *Nat. Commun.* **2015**, *6*, 7961.

(30) Wenger, B.; Nayak, P. K.; Wen, X.; Kesava, S. V.; Noel, N. K.; Snaith, H. J. Consolidation of the Optoelectronic Properties of CH3NH3PbBr3 Perovskite Single Crystals. *Nat. Commun.* **2017**, *8* (1), 590.

(31) deQuilettes, D. W.; Jariwala, S.; Burke, S.; Ziffer, M. E.; Wang, J. T.-W.; Snaith, H. J.; Ginger, D. S. Tracking Photoexcited Carriers in Hybrid Perovskite Semiconductors: Trap-Dominated Spatial Heterogeneity and Diffusion. *ACS Nano* **2017**, *11* (11), 11488−11496.

DOI: 10.1021/acsenergylett.8b00509
ACS Energy Lett. 2018, 3, 1233−1240

(32) Kedem, N.; Kulbak, M.; Brenner, T. M.; Hodes, G.; Cahen, D. Type-Inversion as a Working Mechanism of High Voltage MAPbBr3-(Cl)-Based Halide Perovskite Solar Cells. *Phys. Chem. Chem. Phys.* **2017**, *19* (8), 5753−5762.
(33) Wright, A. D.; Verdi, C.; Milot, R. L.; Eperon, G. E.; Pérez-Osorio, M. A.; Snaith, H. J.; Giustino, F.; Johnston, M. B.; Herz, L. M. Electron−phonon Coupling in Hybrid Lead Halide Perovskites. *Nat. Commun.* **2016**, *7*, 11755.
(34) Herz, L. M. Charge-Carrier Mobilities in Metal Halide Perovskites: Fundamental Mechanisms and Limits. *ACS Energy Lett.* **2017**, *2* (7), 1539−1548.
(35) Shi, D.; Adinolfi, V.; Comin, R.; Yuan, M.; Alarousu, E.; Buin, A.; Chen, Y.; Hoogland, S.; Rothenberger, A.; Katsiev, K. Low Trap-State Density and Long Carrier Diffusion in Organolead Trihalide Perovskite Single Crystals. *Science* **2015**, *347*, 519−522.
(36) Dong, Q.; Fang, Y.; Shao, Y.; Mulligan, P.; Qiu, J.; Cao, L.; Huang, J. Electron-Hole Diffusion Lengths > 175 μm in Solution-Grown $CH_3NH_3PbBr_3$ Single Crystals. *Science* **2015**, *347* (6225), 967−970.
(37) Rehman, W.; McMeekin, D. P.; Patel, J. B.; Milot, R. L.; Johnston, M. B.; Snaith, H. J.; Herz, L. M. Photovoltaic Mixed-Cation Lead Mixed-Halide Perovskites: Links between Crystallinity, Photo-Stability and Electronic Properties. *Energy Environ. Sci.* **2017**, *10* (1), 361−369.
(38) Rehman, W.; Milot, R. L.; Eperon, G. E.; Wehrenfennig, C.; Boland, J. L.; Snaith, H. J.; Johnston, M. B.; Herz, L. M. Charge-Carrier Dynamics and Mobilities in Formamidinium Lead Mixed-Halide Perovskites. *Adv. Mater.* **2015**, *27* (48), 7938−7944.
(39) Habisreutinger, S. N.; Wenger, B.; Snaith, H. J.; Nicholas, R. J. Dopant-Free Planar n−i−p Perovskite Solar Cells with Steady-State Efficiencies Exceeding 18%. *ACS Energy Lett.* **2017**, *2* (3), 622−628.
(40) van Reenen, S.; Kemerink, M.; Snaith, H. J. Modeling Anomalous Hysteresis in Perovskite Solar Cells. *J. Phys. Chem. Lett.* **2015**, *6* (19), 3808−3814.
(41) Hoke, E. T.; Slotcavage, D. J.; Dohner, E. R.; Bowring, A. R.; Karunadasa, H. I.; McGehee, M. D. Reversible Photo-Induced Trap Formation in Mixed-Halide Hybrid Perovskites for Photovoltaics. *Chem. Sci.* **2015**, *6* (1), 613−617.

DOI: 10.1021/acsenergylett.8b00509
ACS Energy Lett. 2018, 3, 1233−1240